IEEE Access
Multidisciplinary ⋮ Rapid Review ⋮ Open Access Journal

Received 7 April 2024, accepted 20 April 2024, date of publication 23 April 2024, date of current version 9 May 2024.

Digital Object Identifier 10.1109/ACCESS.2024.3392768

RESEARCH ARTICLE

Transfer Diagnosis Model of Internal Combustion Engine With Embedded Vibration Signal Impact Decomposition

HE LI[1,2], LIANGYU DONG[3], YANG PENG[4], ZHIXIANG DAI[4], YANG JIANG[5], AND JINJIE ZHANG[1,2]

[1]Key Laboratory of Engine Health Monitoring-Control and Networking Ministry of Education, Beijing University of Chemical Technology, Beijing 100029, China
[2]State Key Laboratory of High-End Compressor and System Technology, Beijing University of Chemical Technology, Beijing 100029, China
[3]China Industrial Control Systems Cyber Emergency Response Team, Beijing 100040, China
[4]Gathering and Transportation Engineering Technology Research Institute, PetroChina Southwest Oil and Gasfield Company, Chengdu 610051, China
[5]Chongqing City Construction Investment (Group) Company Ltd., Chongqing 400015, China

Corresponding author: Jinjie Zhang (zjj87427@163.com)

This work was supported in part by the National Natural Science Foundation of China under Grant 52101343 and Grant 52201351, and in part by the Fundamental Research Funds for the Central Universities under Grant JD2306 and Grant JD2309.

ABSTRACT Traditional transfer diagnosis models for internal combustion engines show a decrease in generalization ability due to the multisource features aliasing in vibration signals and the effect of variable operating conditions. To address this problem, this paper proposes a transfer diagnosis model based on the deep subdomain adaptive network framework. To address feature aliasing, based on minimizing amplitude moment and reconstruction loss, a new adaptive decomposition layer is designed and embedded into the framework to decompose complex signals into single-impact components in time domain. To alleviate the effect of operating conditions, a new constraint for minimizing signal feature variance loss is designed and introduced into the framework's loss function. This constraint calculates the variance of the sample features of the same fault label under variable operating conditions, aiming to excavate invariant features of operating conditions and complete feature mapping of domain adaptation. Validation with experimental data yields an accuracy of 94.81%.

INDEX TERMS Artificial neural networks, deep learning, diesel engines, fault detection, feature extraction, internal combustion engines, signal processing algorithms, time-domain analysis, transfer learning, vibrations.

I. INTRODUCTION

Reciprocating internal combustion engines are the key power source in fields such as marine vessels, vehicles, and electricity generation, characterized by their compact structure, numerous components, and high failure rates. During normal operation, internal combustion engines' shell vibration signals exhibit characteristics of multi-source impact signal coupling. For instance, impacts from the opening and closing of the intake and exhaust valves in each operating cycle, combustion impacts within the cylinder, and impacts from piston reversal. The opening and closing impacts of the valves, combustion impacts within the cylinder, and piston reversal impacts directly affect the cylinder head shell. The piston reversal impact is also transmitted to the cylinder head shell through certain signal paths. Therefore, monitoring the vibration signals of the cylinder head shell of the internal combustion engine can obtain quasi-periodic multi-impact coupling signals in the time domain, thus reflecting the working status of different components. There are many studies extracting fault characteristics from the vibration signals of the cylinder head shell of internal combustion engines and constructing diagnostic models [1], [2].

Mechanical faults, such as wear on connecting rod bearings and valves, produce additional impact signals. These signals overlap with the normal impact signals mentioned

The associate editor coordinating the review of this manuscript and approving it for publication was Gerard-Andre Capolino.

above in the time and frequency domains, posing challenges for fault feature extraction. Meanwhile, variations in engine speed and load conditions are common. Under variable operating conditions, changes occur in the dynamic behavior of engine moving parts, resulting in corresponding changes in the time–frequency features of vibration signals [3], [4]. The features of vibration signals from the engine casing generally exhibit nonlinear distributions during variable operating conditions. Therefore, the feature aliasing and the effects of variable operating conditions are two problems in internal combustion engine fault diagnosis.

To address the problem of feature aliasing, signal modal decomposition methods (i.e., empirical mode decomposition, variational mode decomposition, and wavelet decomposition) are commonly conducted to obtain multiscale single-modal components containing mechanical operational state information [5], [6]. Then the components are applied to extract dynamics and thermodynamic features for diagnosis [7]. For example, Bi et al. [8] used variational mode decomposition and expectation maximization method to analyze multi-channel vibration signals and extract knowledge features for internal combustion engine state recognition. Further, deep learning techniques, including convolutional neural networks [9], [10], [11], graph attention networks [12] and autoencoders [13] are employed to explore the deep features of internal combustion engine vibration signals. For instance, Liang et al. [10] and Xie et al. [11] constructed internal combustion engine vibration signal feature extraction models based on autoencoders and graph attention networks, respectively, using vibration signals directly as input. However, internal combustion engine faults often manifest as abnormal impacts in time domain signals, with a particularly severe feature aliasing problem [15]. The abovementioned research on feature extraction of internal combustion engines did not consider feature aliasing problem and directly used deep networks for feature extraction, resulting in insufficient correlation between feature extraction results and faults, decreased generalization, and limited application.

To alleviate the effect of variable operating conditions, the transfer learning (TL) method has been proposed to further improve the generalization of diagnostic models [16]. TL aims to adjust existing model parameters to construct models that adapt to the diagnostic needs of new engine units. However, the nonlinear variation of signal features under different operating conditions of internal combustion engines makes it challenging to extract domain-invariant features for operating conditions, decreasing the generalization ability of fault transfer diagnostic models between units. Currently, limited research exists on transfer diagnostic models between different internal combustion engine units under variable operating conditions. But in other mechanical domains, such as bearings, gears, and turbines, domain adaptation (DA) methods have been proposed to reduce the feature distribution difference between the source and target domains [17], [18], [19], [20], [21]. DA reduces feature distribution discrepancy by introducing a distance function into the model's objective function to drive multidomain feature alignment [22]. Additionally, incorporating a loss constraint related to label prediction results, combined with the aforementioned feature distribution distance function, DA can reduce the feature distribution difference between the source and target domains while enhancing the diversity of distribution results among multiple classes of source domain features, thereby improving model generalization [23]. Lu et al. [24] used a model with maximum mean discrepancy (MMD) to minimize differences between various machine data instances and achieved an accurate transfer diagnosis of typical gearbox-bearing faults. Shen et al. [25] proposed a deep subdomain adaptation network (DSAN) to extract features of multiscale vibration signals using local maximum mean discrepancy (LMMD) loss to reduce the distance between source and target domains and achieve transfer diagnosis of wind turbine system faults. Li et al. [26] introduced an adversarial DA method based on conditional adversarial DA (CDAN), which enforces better intraclass compactness and interclass separability of label-related prediction results to improve model generalization, enabling transfer diagnosis of typical bearing faults under variable conditions. The above studies have shown that constructing feature distribution constraint functions effectively obtains domain-invariant features under variable operating conditions.

In summary, when constructing internal combustion engine fault transfer diagnostic models, challenges arise such as feature aliasing of vibration multisource impact signals, difficulty in feature extraction, and nonlinear distributions in multidomain feature distribution under variable operating conditions. These challenges lead to difficulty extracting domain-invariant features for operating conditions and a decrease in the generalization ability of fault transfer diagnostic models between engine units.

In this study, first, to address the difficulty in feature extraction caused by feature aliasing, a new decomposition layer of multi-impact vibration signals in internal combustion engines is proposed. This layer is based on the periodic multi-impact interval distribution and rapid decay characteristics of impacts in vibration signals. This proposed layer has a signal moment minimization decomposition objective, enabling the decomposition of multisource impact vibration signals into single-impact modalities. Second, to address the problem of signal feature shift under variable operating conditions, which makes it challenging to mine domain-invariant features, a new feature variance loss (FVL) constraint is established. By introducing source domain labels to group source domain samples and calculating the variance of each feature under all operating conditions, this constraint drives the minimization of the variance of feature distribution for different operating condition subsignals with the same fault label, reducing the sensitivity of sample features to operating conditions. Furthermore, the decomposition layer of the impact vibration signals and the FVL constraint are inte-

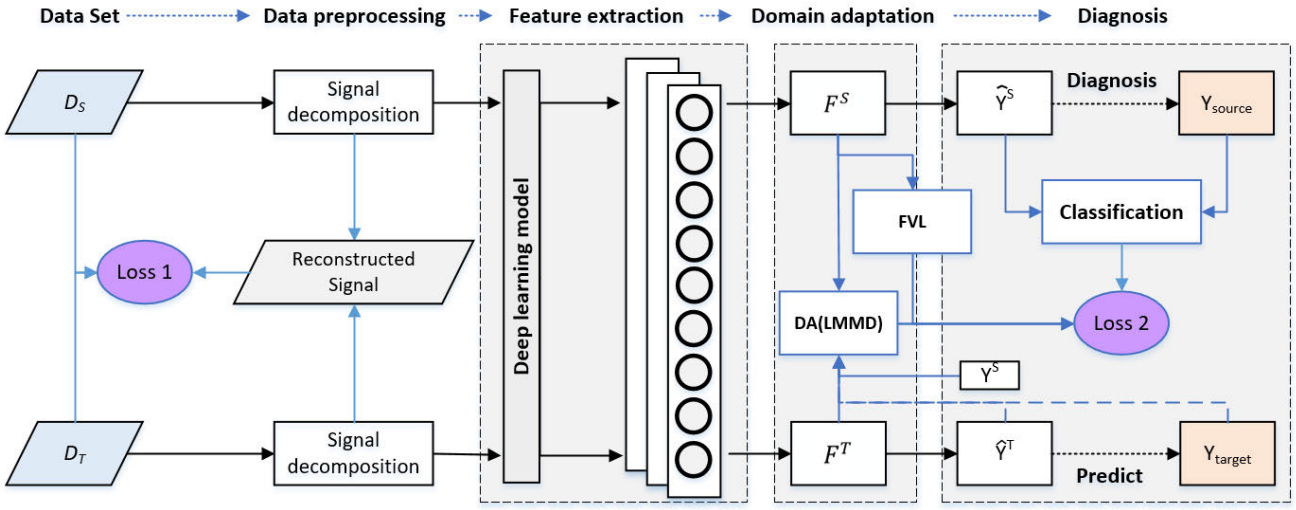

FIGURE 1. Framework of the proposed method is based on signal decomposition, feature extraction, domain adaptation, and diagnostic modules.

grated into the signal processing and DA modules of the DSAN framework, respectively. This integration leads to the construction of a DSAN framework for internal combustion engine transfer diagnosis, enabling fault transfer diagnosis between internal combustion engine units.

Our contributions are as follows:

1. Proposed a new decomposition layer based on signal amplitude moment and reconstruction loss minimization of internal combustion engine vibration signals, and the signal moment minimization decomposition objective. This layer is embedded in DSANs and decomposes multiple impact signals into single-impact modes. It also adopts a unified optimization algorithm, parameter update strategy, and learning rate adjustment method with other modules in the model to improve the model efficiency.

2. Proposed a new FVL constraint to mine invariant features in the operating condition domain. This constraint introduces source domain labels to group source domain samples and calculates the variance of each feature under all operating conditions, driving the minimization of the variance of feature distribution for different operating condition subsignals with the same fault label to reduce the sensitivity of sample features to operating conditions.

3. Constructed a new internal combustion engine transfer diagnostic model based on a DSAN framework. This framework incorporates the proposed multi-impact vibration signal decomposition layer and FVL constraint and establishes an algorithm for multiobjective optimization of the model.

4. Based on experiments conducted on two internal combustion engine test benches, simulating three typical faults under different operating conditions, the performance of the proposed model is validated.

The remaining content of this study is as follows: Chapter 2 presents the proposed decomposition layer, the FVL, and the constructed transfer diagnostic model. Chapter 3 describes the experiments and the data set. Chapter 4 presents the comparative validation results of the proposed method, and Chapter 5 provides the conclusions of our study.

II. PROPOSED METHOD

This study constructed a DSAN framework for the internal combustion engine transfer diagnosis model with embedded vibration signal impact decomposition, and Figure 1 shows the model's overall structure. This structure included a preprocessing module for the signal decomposition layer, a feature extraction module, a DA module with the proposed embedded FVL, and a fault diagnosis module.

A. DECOMPOSITION LAYER OF MULTI-IMPACT VIBRATION SIGNALS

The decomposition layer aims to separate the impulse waveforms within the vibration signal, forming multiple subsignals containing only individual impulse waveforms. Its decomposition objective can be summarized as minimizing the information loss in reconstructing the source signal, with the subsignals conforming to the morphology of single impulse waveforms [1]. Additionally, for ease of calculation, the signal amplitude and time range need to be transformed to [0,1], and after decomposition, inverse transformation can restore the original feature range.

The design of the decomposition window and the calculation process of window parameters are as follows.

To construct the decomposition window W, we defined the center position coefficient (w_c) and half-width coefficient (w_l). Window W comprises variants of *Sigmoid* and *ReLU* functions. Multiplying the signal S by W intercepts the signal, as shown in Eqs. (1)–(2).

$$F_g(w_c, w_l; x)$$

$$= \frac{1}{1 + \exp\left(w_c - w_l - x\right)} \tag{1}$$

$$W\left(w_c, w_l; x\right) = \mathrm{ReLU}\left(F_g\left(w_c, w_l; x\right) - F_g\left(w_c, -w_l; x\right) - \varepsilon\right), \tag{2}$$

where F_g is the sigmoid activation function of the variant. ReLU is the standard activation function. The x represents the time point of the sequence. ε represents a minimum value, usually taken as 10^{-4}.

The formula for calculating (w_c) and (w_l) are shown in Eqs. (3)-(4).

$$w_c = \mathrm{sigmoid}\left(w'_{w_c} S\right) \tag{3}$$

$$w_l = \mathrm{sigmoid}\left(w'_{w_l} S\right), \tag{4}$$

where w_c and w_l are generated by deep learning weights w'_{w_c} and w'_{w_l}, respectively.

The calculation process of subsignals is shown in Eq. (5)

$$s_k\left(x\right) = W_k\left(w_{c_k}, w_{l_k}; x\right) S\left(x\right), \tag{5}$$

where $s_k\left(x\right)$ represents the separately decomposed subsignals. k represents the index of the decomposed subsignals, and $S\left(x\right)$ represents the source signal.

The decomposition objectives are as follows.

Considering that the decomposition target needs to minimize the information loss of the reconstructed source signal, the decomposition and reconstruction loss δ is proposed as an indicator to evaluate the decomposition performance. As shown in in Eq. (6).

$$\delta = \frac{1}{K}\left(\sum_{k=1}^{K} s_k\left(x\right) - S\left(x\right)\right)^2, \tag{6}$$

where K represents the number of decompositions

Considering the morphological characteristics of a single impact waveform, the decomposition layer introduces the concepts of impact amplitude moment and impact time domain center.

The p-th amplitude moment of signal $s\left(x\right)$ for a certain moment (x_k) is shown in Eq. (7).

$$M_t\left(x|x_k, s\left(x\right), p\right) = \int_0^{+\infty} \left(x - x_k\right)^p s\left(x\right) dx, \tag{7}$$

where the M_t represents the amplitude moment. When (x_k) is the time center of gravity of the signal $s\left(x\right)$, the amplitude moment reaches its minimum value at point (x_k). In this study, under the condition of $p = 1$, (x_k) represents the time domain center of the signal s in the time domain.

The smaller the reconstruction loss, the less information lost during decomposition. The smaller the amplitude moment M, the closer x_k is to the true time domain center of the impulse waveform. The decomposition target is shown in Eq. (8).

$$\min_{\{s_k\},(t_k)} \mathcal{L}_D = \delta + \beta \sum_{k=1}^{K} M_t\left(x \mid x_k, s_k(x), p = 1\right)_2^2 \tag{8}$$

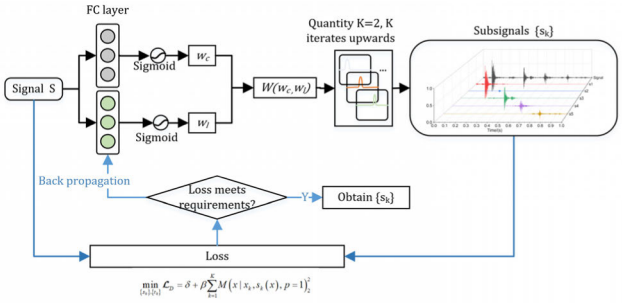

FIGURE 2. Schematic diagram of decomposition layer for multi-impact vibration signals.

where $\mathcal{L}_D$ represents the decomposition target, and the β represents the adjustment coefficient.

The optimization calculation process for the decomposition number K is as follows. This study sets the decomposition number K to start from two and iteratively calculates upward. When the decomposition target $\mathcal{L}_D$ is the smallest, the value of K is the optimum.

The proposed signal decomposition layer is shown in Figure 2.

Embed the above signal decomposition layer into the DSAN framework. Compared to conventional decomposition methods that are independent of diagnostic networks for signal decomposition, the signal decomposition layer in this study utilizes the common Adam optimization algorithm in deep learning. This maintains the same parameter update strategy and learning rate adjustment method as other modules in the framework, thereby improving the efficiency of the transfer diagnosis model.

B. FEATURE VARIANCE LOSS

In the current study, computing feature variance has been utilized in model regularization loss to drive the model to generate feature distributions closer to both the existing training set and unobserved real-world data, thereby enhancing model generalization [27]. The proposed FVL in this paper further incorporates information on operating conditions and fault labels for sample grouping, aiming to reduce the sensitivity of the model's feature extraction results to operating conditions. It should be pointed out that FVL loss is applied to the DA module and works together with the distance function of the DA module itself.

The rationale for introducing labels is as follows. Although minimizing the variance of feature dimensions calculated from samples under different operating conditions can decrease the feature variation caused by operating conditions, the prerequisite for minimizing the variance of feature dimensions is sampled with the same fault label, given that the samples required during model training are randomly selected. Otherwise, the reduction in feature variance for samples with different fault labels will result in similar feature values, making fault diagnosis difficult for the model.

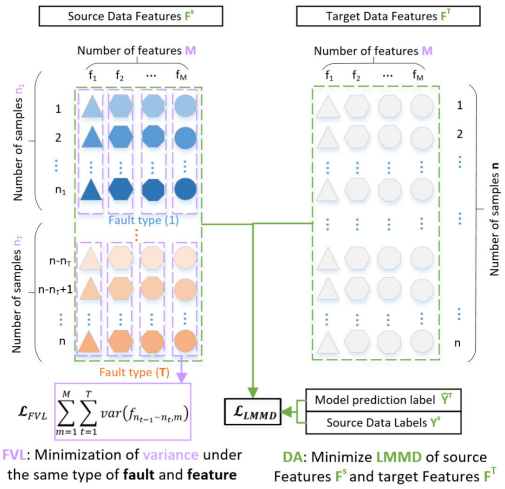

FIGURE 3. Schematic diagram of using FVL to reduce the impact of variable operating conditions in the DA process.

Therefore, FVL groups the source domain samples by introducing label information. Furthermore, based on the pre-grouped samples and the fault label information from the source domain, FVL calculates the variance of each feature under all operating conditions, driving the minimization of the variance of feature distribution for different operating condition sub-signals with the same fault label, (i.e., minimizing the sensitivity of features to operating conditions).

Consider a batch of samples with n samples containing T classes of faults. The number of samples for each class of fault is n_t, and each sample has M deep learning features, as shown in Eq. (9).

$$F = \left\{f_{i,j}\right\}, F \in \mathbb{R}^{\left(\sum_{t=1}^{T} n_t\right)*m}, \tag{9}$$

where F represents the total feature matrix for a batch of samples, the $f_{i,j}$ represents the j-th feature of the i-th sample, n is the total number of samples in a batch, and $n_t$represents the number of samples for the t-th class of fault.

For features belonging to the same fault class, the goal is to minimize feature variance, which drives the model to learn noise features as zero features. Therefore, the variance-based penalty constraint is as shown in Eq. (10).

$$\mathcal{L}_{FVL} = \min_{W_E} \frac{1}{MT} \sum_{m=1}^{M} \sum_{t=1}^{T} \text{var}\left(f_{n_{t-1}\sim n_t,m}\right), \tag{10}$$

where *var* represents variance calculation, T and M represent the number of fault and feature categories, respectively, $f_{n_t-1\sim n_t,m}$ is the m-th feature of samples from $n_t-1 \sim n_t$, and W_E represents the weights generated in the feature process.

After feature extraction, further evaluation of each feature dimension in the feature map is required. If any feature value in a dimension is zero, that feature dimension will be removed.

The process of DA with FVL is shown in Figure 3.

C. MODEL FRAMEWORK FOR TRANSFER LEARNING

This study adopts a DSAN framework to achieve transfer fault diagnosis, embedding the proposed signal decomposition layer and FVL constraint. The feature extraction module of the framework consists of the classical VGG structure [28], while the DA module employs LMMD as the distance loss function. For the diagnostic module, a classical softmax classifier is applied.

LMMD aims to drive the alignment of sample features in each subdomain. Usually, the source domain data are divided into subdomains based on class labels, whereas the target domain data is divided into subdomains using the probability distribution predicted by the network. The definition of LMMD is shown in Eqs. (11)-(12).

$$w_i^c = \frac{y_{ic}}{\sum_{(x_j,y_j)\in D} y_{ic}} \tag{11}$$

$$\mathcal{L}_{LMMD} = \frac{1}{T}\sum_{c=1}^{T} \times \left\| \sum_{x_i^s \in D^S} w_i^{sc} \phi\left(x_i^s\right) - \sum_{x_j^t \in D^T} w_j^{tc} \phi\left(x_j^t\right) \right\|_H^2, \tag{12}$$

where, D^S and D^T represent the feature matrix of the source and target domain, respectively, T is the number of classifications, and ϕ represents a kernel function, such as a Gaussian kernel.

The softmax classifier is a classical classifier used for multiclass classification, with focal loss ($\mathcal{L}_{FL}$) as the diagnostic target for unbalanced data. $\mathcal{L}_{FL}$ is shown in Eq. (13).

$$\mathcal{L}_{FL}\left(p_{t,i}\right) = -\alpha_i \left(1 - p_{t,i}\right)^{\gamma} \log\left(p_{t,i}\right), \tag{13}$$

where $p_{t,i}$ is the cross-entropy loss between the predicted probability of class i and the true label. Factor α is a used to adjust the weight of each category. Factor γ is a used to adjust the weight relationship between samples.

The objective function comprises three learning tasks, which can be divided into the preprocessing part $\mathcal{T}_1$, the FVL part $\mathcal{T}_2$, and the diagnostic part $\mathcal{T}_3$, as shown in Eqs. (14)-(16).

$$\mathcal{T}_1 = \mathcal{L}_D \tag{14}$$

$$\mathcal{T}_2 = \mathcal{L}_{FVL} \tag{15}$$

$$\mathcal{T}_3 = \lambda\mathcal{L}_{LMMD} + \mathcal{L}_{FL}, \tag{16}$$

where λ is the balancing coefficient.

For these three learning tasks, a multiobjective stepwise training method was designed. First, the source and target domain data were trained using a multi-impact vibration signal decomposition layer to achieve signal decomposition based on the minimization objective $\mathcal{T}_1$. After training, the decomposed source domain signals were further grouped and trained, primarily driving the model parameters to acquire domain-invariant features for operating conditions by minimizing the $\mathcal{T}_2$. Subsequently, DA and diagnosis were performed on both the source and target domain data,

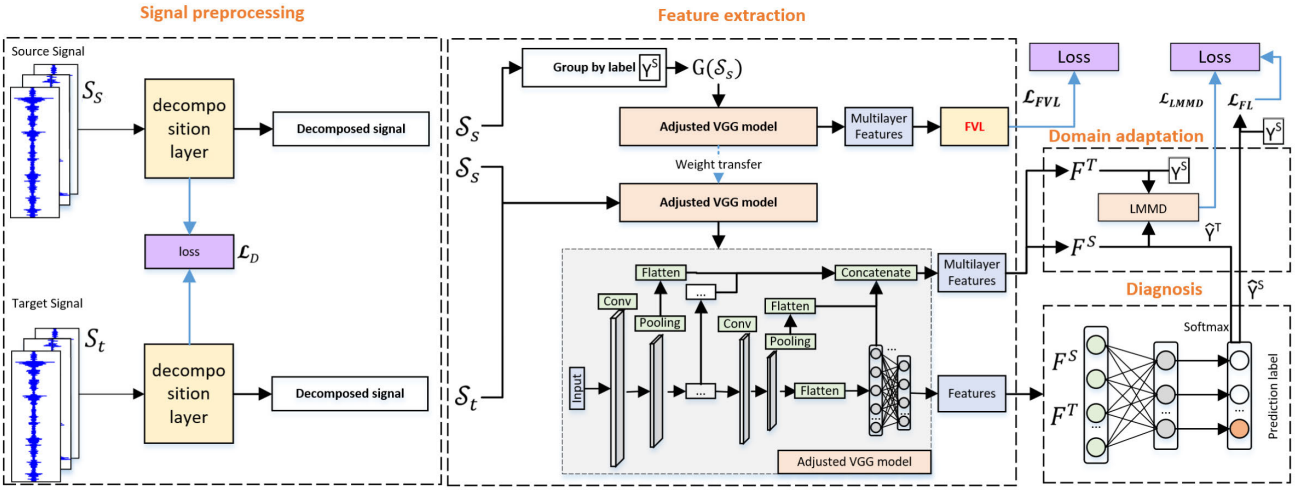

FIGURE 4. Specific framework of the proposed method based on signal decomposition layer, feature extraction, domain adaptation, and diagnostic modules.

Algorithm 1 Proposed Transfer Learning Model

Input: source data S_S, source label Y_s, target data S_t, task $\mathcal{T}_1$ and its threshold ψ_1, limit of epochs L_{ep1}, task $\mathcal{T}_3$ and its thresholdψ_3, limit of epochs L_{ep2}
Output: Predict the results of target data $\hat{y}_t$

```
Epoch=0
While T_1 > ψ_1 or Epoch < L_ep1 do
    Based on S_s, S_t, train decomposition layer with task T_1 = L_D
    Epoch = Epoch+1
end while
Obtain the subsignals set S_s, S_t of S_S, S_T
Based on S_s and y_s, group S_s as G(S_s)
Epoch=0
While T_3 > ψ_3 or Epoch < L_ep2 do
    Based on the transfer learning model (Model), calculate F^S of G(S_s) with minimize task T_2 = L_FVL
    Based on Model, source label Y_s, calculate F^S, F^T, Ŷ^T of S_s, S_t, with minimize L_LMMD
    Based on F^S and source label Y_s, conduct classification diagnosis with minimize L_FL
    Task T_3 = λ L_LMMD + L_FL
    Epoch = Epoch+1
end while
Based on the trained model and target data S_t, predict the results of target data ŷ_t
```

(i.e., adjusting the model parameters by minimizing objective $\mathcal{T}_3$). The model then alternately underwent training to minimize objectives $\mathcal{T}_2$ and $\mathcal{T}_3$ until objective $\mathcal{T}_3$ met the requirements.

Furthermore, the training approach for the model is defined by Algorithm 1 below, and the specific model structure is illustrated in Figure 4.

TABLE 1. Sample collection results for the two internal combustion engines.

Unit	Structure	Rotation	Load	Fault type-abbreviation	Number of samples
A	12-cylinder V-type	1000–1500 rpm	0–400 Nm	Normal(T1)	1100
				Misfire(T2)	1100
				Valve fault(T3)	1100
			0 Nm	Collision(T4)	25
B	6-cylinder Inline-type	1000–1800 rpm	0–400 Nm	Normal(T1)	1100
				Misfire(T2)	360
				Valve fault(T3)	360
			0 Nm	Collision(T4)	25

III. DATA AND MODEL

A. DATA

To validate the transfer diagnostic effectiveness of the proposed method, experiments were conducted involving combustion engine misfires, abnormal valve clearance, and piston collision faults. The misfire fault was achieved by manually cutting off combustion injection into the cylinder, the abnormal valve clearance was introduced by manually adjusting the exhaust valve clearance to increase it by +0.3 mm, and the piston collision fault was created by adding soft copper sheets to the piston head. The source domain data were obtained from a 12-cylinder V-type direct-injection combustion engine, referred to as Group A, whereas the target domain data were obtained from a 6-cylinder Inline-type direct-injection combustion engine, referred to as Group B. The fault experiments on Groups A and B are shown in Figure 5. The sample collection results are shown in Table 1.

In Figure 5, the green symbol represents the vibration acceleration sensor installed on the cylinder head to obtain vibration signals. The number and location of sensors may vary depending on the unit structure and installation location

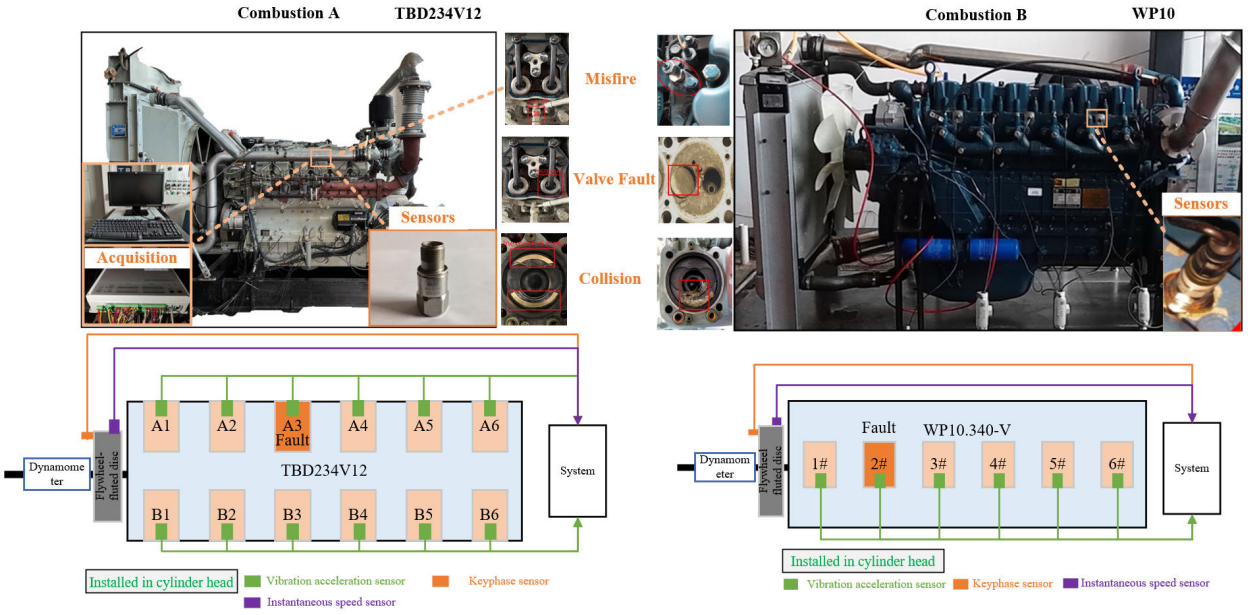

FIGURE 5. Structure of internal combustion engines (unit A and unit B), layout of engine measuring points and installation locations of engine sensors.

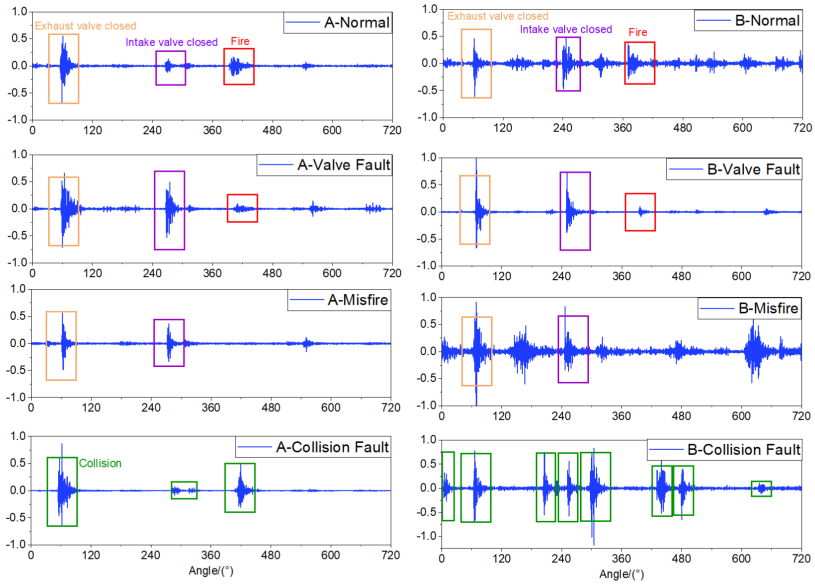

FIGURE 6. Schematic diagram of vibration signals for normal, misfire, valve, and collision faults in Unit A and Unit B.

conditions. Unit A has installed 12 sensors of this type parallel to the direction of the piston application on the cylinder head; Unit B installed 6 sensors of this type on the cylinder head perpendicular to the direction of the piston operation. The orange symbol represents the key phase sensor, installed on the flywheel to intercept the vibration signal of one working cycle; the Purple symbol represents the instantaneous speed sensor, used to obtain the operating condition label. The key phase sensor (parallel to the flywheel axis) and instantaneous speed sensor (perpendicular to the flywheel axis) of both units are installed on the flywheel fluted-disc structure. The key phase sensor is used to capture vibration signals of a complete working cycle, while the instantaneous speed sensor is used to obtain operating condition labels. The faulty cylinders of Units A (faulty cylinder A3) and B (faulty cylinder 2#) are used to collect vibration signal samples. These samples are applied as the training and validation dataset for the proposed method.

To better collect high-frequency vibration information caused by mechanical faults, the sampling frequency was set to 25.6 kHz during our experiment (the sensor manual recommends the highest sampling rate). The sample signals are shown in Figure 6.

As shown in Table 1 and Figure 6, the experiments for Group A were distributed between 1000–1500 rpm and 0–400 Nm, while Group B covered the range of 1000–1800 rpm and 0–600 Nm, complying with variable-condition criteria. Observing the vibration signal samples from both groups, the signals from Group A are clearer, with distinct impacts from valve seating and ignition. However, the signals from Group B exhibited numerous unidentified impacts. Our sensor has a sampling frequency of 25.6 kHz and collected data from 1000–1800 rpm. Given that a complete working cycle of an internal combustion engine requires the main shaft to rotate twice, the number of sampling sequence points for a sample is 1700–3072. To minimize information loss, a sampling number of 3072 is taken as the interpolation length of the overall signal.

B. MODEL

The model constructed here includes four modules or methods: the signal decomposition layer for signal preprocessing, the modified VGG module for feature extraction and diagnosis, the LMMD method for DA, and the FVL method for feature selection.

The parameters of the modified VGG module are shown in Table 2. The model structure and parameters refer to the commonly used VGG structure [28]. It should be noted that for calculation convenience, the length of the input signal in this article was uniformly interpolated to 3072, and the training method used was train-on-batch, which randomly extracts a batch of samples from the dataset for one-step training. Therefore, the K value depends on the maximum number of decompositions of the input signal in a dataset after being decomposed by the signal decomposition layer, and the remaining signals are zeroed to satisfy the same shape of a batch input signal (3072, K).For calculation convenience, the length of the input signal in this article was uniformly interpolated to 3,072, and the training method used was train-on-batch, which randomly extracts a batch of samples from the dataset for one-step training. Therefore, the K value depends on the maximum number of decompositions of the input signal in a dataset after being decomposed by the signal decomposition layer, and the remaining signals are zeroed to satisfy the same shape of a batch input signal (3072, K).

It should be pointed out that the parameter settings in Table 3 are based on the following criteria.

Referring to the [1], the parameter "p" was set to "1" in the signal decomposition layer, which has been validated by actual vibration signal cases of internal combustion engines. Referring to the [29], γ was set to "2" to focus the model more on difficult-to-classify samples. Since the dataset contains four states: normal, misfire, valve fault, and collision,

TABLE 2. Structure of VGG in the transfer diagnosis model.

Block	Details	Output size
Input	(3072, K)	(Batch,3072, K,1)
Block1	Conv3-64	(Batch, 3072, K, 64)
	Max-pool	(Batch,768, K, 64)
Block2	Conv3-128	(Batch, 768, K, 128)
	Max-pool	(Batch,384, K, 128)
Block3	Conv3-256	(Batch, 384, K, 256)
	Conv3-256	(Batch, 384, K, 256)
	Max-pool	(Batch,192, K, 256)
Block4	Conv3-512	(Batch,192, K, 512)
	Conv3-512	(Batch,192, K, 512)
	Max-pool	(Batch,81, K, 512)
Block5	Conv3-512	(Batch, 81, K, 512)
	Conv3-512	(Batch, 81, K, 512)
	Global-Max-pool	(Batch, 512)
Fully connected layer (FC)	FC-128	(Batch,128)
	FC-32	(Batch,32)
Classifier	FC-4	(Batch,4)

TABLE 3. Each module and its parameter values in the transfer diagnosis model.

Module	Parameters	Value
Signal decomposition layer	p	1
	ψ_1	0.01
	L_{ep1}	100
	batch	64
Modified VGG	ψ_3	0.05
	L_{ep2}	2000
$\mathcal{L}_{FL}$	α	Total number of samples / (Number of classifications × The number of samples in calculated classification)
	γ	2
$\mathcal{L}_{LMMD}, \mathcal{L}_{FVL}$	T	4
Balancing coefficient	λ	0.1

the parameter "T" was set to "4". The balancing coefficient λ was set to balance the numerical magnitudes of various loss terms in the total loss function of the model. Under the conditions of the dataset used in this study, setting the parameter "λ" to "0.1" can ensure that the specific values of $\mathcal{L}_{LMMD}$ and $\mathcal{L}_{FL}$ differ within one order of magnitude during the training process.

In addition, the settings for the number of signal decomposition and transfer training epochs thresholds L_{ep1}, L_{ep2}, and the model signal decomposition and transfer task loss thresholds ψ_1, ψ_3, were determined based on multiple training iterations of the model. These settings were based on the convergence range of the model's final loss (loss fluctuating around a certain value) and the number of training steps required to reach this convergence threshold, selecting a set of parameter values suitable for the dataset used in this study.

IV. RESULTS

A. EFFECT OF THE DECOMPOSITION LAYER OF MULTI-IMPACT VIBRATION SIGNALS

This study measured the decomposition effectiveness using the decomposition metrics. The reconstruction energy loss

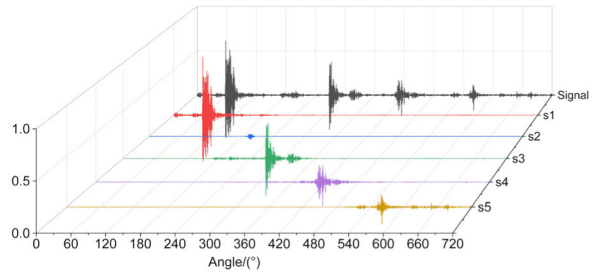

FIGURE 7. Decomposition results of a cylinder valve fault sample of the source unit.

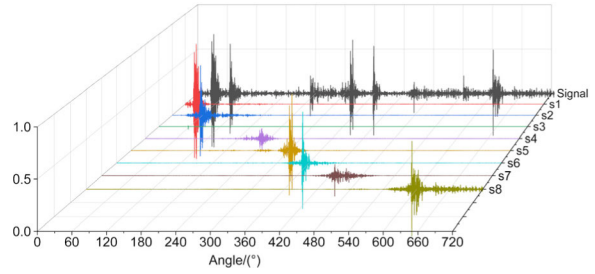

FIGURE 8. Decomposition results of a cylinder collision fault sample of the target unit.

TABLE 4. Average decomposition metrics (EL and ol) of unit A and unit b.

Data	EL	OL
A unit	1.54%	0.023
B unit	2.72%	0.028

(EL) and orthogonal loss (OL) coefficient between the decomposed subsignals were provided as a metric for assessing the decomposition method, as shown in Eqs. (17)–(18).

$$\mathrm{EL} = \frac{\left|\mathrm{RMS}\left(\sum_{i=1}^{K} s_i\left(t\right)\right) - \mathrm{RMS}\left(S\left(t\right)\right)\right|}{\mathrm{RMS}\left(S\left(t\right)\right)} * 100\% \quad (17)$$

$$\cos_{i,j} = \frac{\left|\left\langle s_i(t), s_j(t)\right\rangle\right|}{\left\|s_i(t)\right\|_2 \left\|s_j(t)\right\|_2}, s_i(t), s_j(t) \in \left\{s_k(t)\right\},$$

$$\mathrm{OL} = \frac{1}{K(K-1)}\left(\sum_{i=1}^{K}\sum_{j=1}^{K}\cos_{i,j} - K\right), \quad (18)$$

where EL represents the reconstruction energy loss between the decomposed and original signals, RMS represents the root-mean-square value, and OL reflects the orthogonal loss between each subsignal. The smaller OL represents better orthogonality.

Taking a valve fault sample of the source unit and a cylinder collision fault sample of the target unit as examples, the decomposition results are shown in Figures 7 and 8, and the indicators are shown in Table 4.

Table 4 shows that the proposed method achieves an average reconstruction EL of 1.54% and an OL of 0.023 on Unit A and an average reconstruction EL of 2.72% and an OL of 0.028 on Unit B.

TABLE 5. Effect of FVL on zero features ratio and feature variance.

Method	Zero feature ratio	Same fault label, average feature variance of operating conditions
Without the FVL	62.50%	0.026
With the FVL	84.38%	0.011

B. EFFECT OF THE FVL

The proposed FVL drives the minimization of the same feature variances under the same fault conditions reflected in the fault-related feature maps. Specifically, it reduces the number of valid features and increases the number of zero features. Zero features can be compressed (squeezed) and omitted in the DA, which helps reduce the dimensionality of DA calculations.

The comparative process is as follows: Using the VGG model, the $\mathcal{L}_{FVL}$ loss was introduced in the feature layers. Diagnostic classification and visualization of feature maps were performed using the decomposed signal set from Group A. The proportion of zero features to the total number of features was then calculated to verify the increase in zero features and the decrease in valid features introduced by $\mathcal{L}_{FVL}$. Figure 9 depicts the visualized results after taking the absolute value of the feature maps in one training process.

Based on the decomposed signal set from Group A, Figure 9 and Table 5 reveal that introducing FVL increased the proportion of zero features from 62.50% to 84.38% and decreased average feature variance from 0.026 to 0.011 under the same fault-operating condition.

C. ABLATION EXPERIMENTS USING THE PROPOSED METHOD

The previous section verified FVL role in feature selection and in limiting the number of features. We conducted ablation experiments to further validate the effectiveness of the remaining parts of the constructed diagnostic model. As shown in Figure 4, after all sample signals are decomposed using the signal decomposition layer, the structure of each part of the proposed model can be simplified, as shown in Figure 10.

The VGG model was used as the feature extraction module, with $\mathcal{L}_{LMMD}$ employed as the target loss function and FVL introduced to enhance DA. Softmax was used as the classifier and label predictor.

According to Table 6, retaining only VGG for training and transfer diagnosis resulted in a diagnostic accuracy of only 24.98% and an F1 score of only 24.19% for the target internal combustion unit, indicating poor diagnostic performance. However, retaining the signal decomposition layer + VGG for training and transfer diagnosis resulted in diagnostic accuracy of only 48.95% and an F1 score of only 32.41% for the target internal combustion unit, indicating poor diagnostic performance. After introducing only LMMD in VGG, the diagnostic results of the target domain significantly

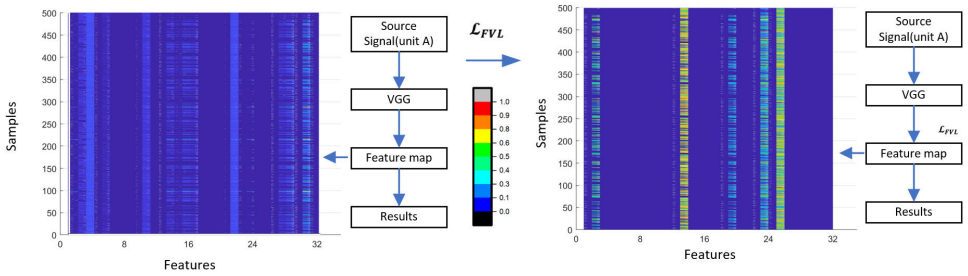

FIGURE 9. Introduction of FVL increased the proportion of zero features and decreased average feature variance under same fault-operating condition label in the signal feature map.

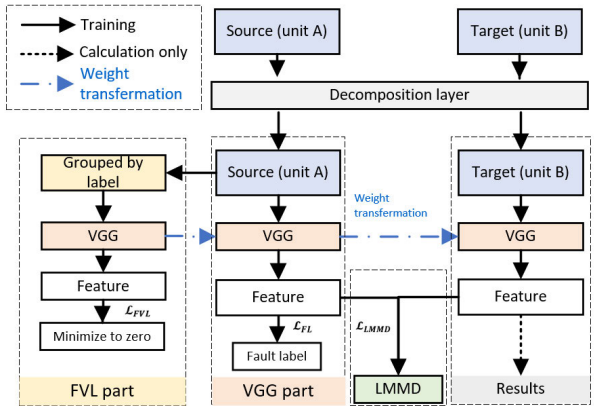

FIGURE 10. Structure of the proposed method using the decomposition layer for signal decomposition, VGG as the feature extraction module, FVL for feature optimization, and LMMD for domain adaptation.

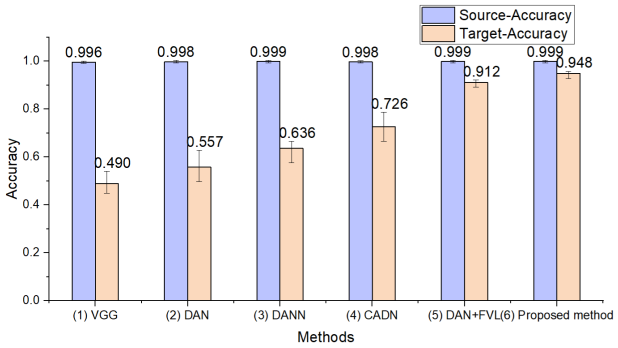

FIGURE 11. Comparison of the accuracy obtained from VGG, DAN, DANN, CDAN, DAN+FVL, and the proposed method.

TABLE 6. Ablation experiments results of proposed transfer diagnosis model.

Method	Accuracy		F1-score (Macro-average)	
	Source domain (unit A)	Target domain (unit B)	Source domain (unit A)	Target domain (unit B)
VGG	97.33%	24.98%	96.21%	24.19%
Decomposition layer +VGG	99.61%	48.95%	99.01%	32.41%
Decomposition layer +VGG+ LMMD	99.67%	93.44%	99.03%	93.17%
Decomposition layer +VGG+LMMD +FVL	99.85%	94.81%	99.08%	94.42%

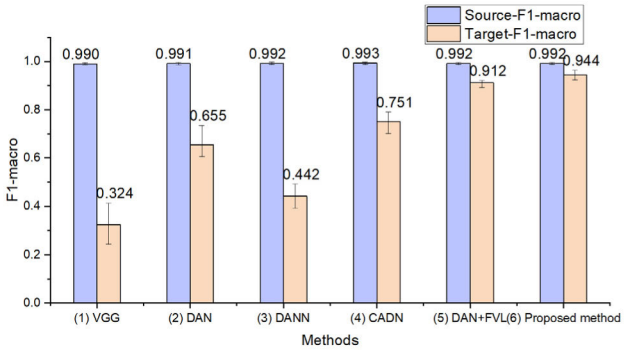

FIGURE 12. Comparison of the F1 scores obtained from VGG, DAN, DANN, CDAN, DAN+FVL, and the proposed method.

improved, achieving an accuracy of 93.44% and an F1 score of 93.17%. Furthermore, after introducing LMMD, VGG further introduced FVL to optimize the features of the input MMD, achieving an accuracy of 94.81% and an F1 score of 94.42%, improving the diagnostic results.

D. COMPARISON WITH OTHER METHODS

To validate the effectiveness of the proposed model in both diagnosis and DA—to achieve effective transfer fault diagnosis for combustion engines under varying operating conditions—we selected the samples from Table 1, with 80% used for training and 20% used for testing in both source and target domains. Furthermore, the following typical methods were employed for comparison:

1) VGG: VGG is a classic convolutional deep learning model. This study used the VGG11 model, which was retrained using the source domain training dataset and transferred to the target domain training dataset using a freeze-tune approach.

2) DAN: For comparison, this study used the VGG11 model as the feature extraction module, and MMD was added

FIGURE 13. Confusion matrix diagram of the diagnostic results for normal(T1), misfire(T2), valve-fault(T3), and collision(T4) faults in the target domain internal combustion engine:(a) Confusion matrix of VGG, (b) Confusion matrix of DAN, (c) Confusion matrix of DANN, (d) Confusion matrix of CDAN, (e) Confusion matrix of DAN+FVL, (f) Confusion matrix of proposed method.

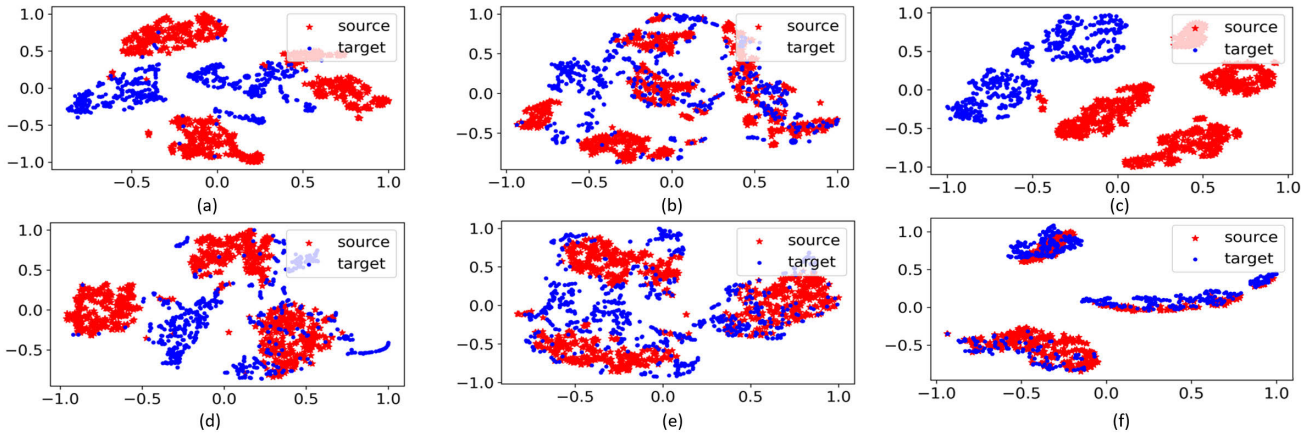

FIGURE 14. TSNE visualization results of source and target domain data features in the feature space: (a) Visualization results of VGG, (b) Visualization results of DAN, (c) Visualization results of DANN, (d) Visualization results of CDAN, (e) Visualization results of DAN+FVL, (f) Visualization results of proposed method.

to the VGG11 model feature layers for DA, thereby constructing the DAN model.

3) DANN: This model includes a feature extractor that maps data to a specific feature space, a label predictor that classifies data from the source domain, and a domain discriminator that classifies data in the feature space. This study used the VGG11 model as the feature extraction module and a gradient reversal layer to build the domain discriminator.

4) CDAN: CDAN employs two novel conditional adjustment strategies—multilinear and entropy—to enhance DA. For comparison, this study used the VGG11 model as the feature extraction module for CDAN.

TABLE 7. Results of the various methods used in the present study.

Method	Accuracy		F1-score		Time	
	Source domain (unit A)	Target domain (unit B)	Source domain (unit A)	Target domain (unit B)	Training	Diagnosis
VGG[28]	99.61%	48.95%	99.01%	32.41%	684s	15.4s
DAN[24]	99.82%	55.73%	99.12%	65.51%	1087s	16.1s
DANN [18]	99.88%	63.57%	99.22%	44.20%	1292s	16.7s
CDAN [26]	99.75%	72.64%	99.29%	75.10%	1547s	20.3s
DAN+FVL	99.87%	91.20%	99.16%	91.16%	1109s	16.0s
Proposed method	99.85%	94.81%	99.08%	94.42%	1053s	16.1s

5) DAN + FVL: This study used the VGG11 model as the feature extraction module. FVL was introduced to enhance the DA process with the MMD function. Softmax was used as the classifier and label predictor.

6) Proposed method: This study used the VGG11 model as the feature extraction module. FVL was introduced to enhance the DA process with the LMMD function. Softmax was used as the classifier and label predictor.

Considering the data sample imbalance between the source (Unit A) and target (Unit B) domains, accuracy and F1-score (Macroaverage) were selected as the evaluation metrics to further demonstrate the performance of the aforementioned methods. The evaluation was conducted over 10 iterations to comprehensively assess the diagnostic performance of these methods, as shown in Table 7 and Figures 11 and 12.

Table 7 and Figures 11 and 12 show that all diagnostic models constructed by these methods could recognize the source domain A-group test data and the training time for all methods is acceptable. However, the effectiveness of the VGG, DAN, DANN, CDAN, and DAN + FVL methods for the target domain B-group dropped significantly (below 80%), with only the proposed method maintaining an accuracy of 94.81% and an F1-score of 94.42%.

To further analyze the reasons for this phenomenon, we extracted the results from a single training run for each method and displayed their structural differences. Specific diagnostic results based on confusion matrices, and feature visualization based on t-distributed stochastic neighbor embedding (t-SNE) are presented in Figure 13 and Figure 14.

From the confusion matrix perspective, the sharp drop in fault recognition performance can be attributed to the difficulty in clearly distinguishing between normal and misfire samples in the target domain group. This phenomenon is exhibited to varying degrees in VGG, DAN, DANN, CDAN, DAN + FVL, and the proposed method. The VGG and DANN methods further undermine the overall fault recognition performance due to their inability to identify knocking. Consequently, the proposed method exhibits the strongest recognition performance.

From a feature visualization clustering perspective, both VGG and DANN show a lack of overlap between the source domain and target domain data in the feature space. The proposed method has a better overlap compared to any other method in this paper. In summary, the above findings validate the effectiveness of the proposed method in transfer diagnosis.

V. CONCLUSION

This study proposes a new model for transfer diagnosis of internal combustion engines based on a DSAN framework, achieving transfer diagnosis between different internal combustion engine units under variable operating conditions.

First, a new multi-impact vibration signal decomposition layer is designed to minimize the signal moment to decompose multiple impact signals into single-impact modes, thereby alleviating the problem of feature aliasing in internal combustion engine vibration signals and extracting signal features rich in equipment operating state information. Second, the FVL constraint is proposed to calculate the feature variance under all operating conditions. This drives the minimization of the feature variance distribution of different operating condition subsignal features with the same fault label, reducing the sensitivity of sample features to operating conditions and exploring domain-invariant features. Third, the proposed vibration signal decomposition layer and domain FVL constraint are embedded based on the DSAN framework to construct the transfer diagnosis model. Finally, four fault experiments were conducted on the V12 high-power internal combustion engine test bench, and the same experiments were replicated on another V6 high-power internal combustion engine test bench, serving as the target domain for transfer. The experiments validated that the proposed model achieved an accuracy of 94.81% and an F1 score of 94.42% in the target domain under variable operating conditions, confirming the transfer diagnostic performance of the proposed method.

However, our proposed method has limitations. For example, it can only identify fault types existing in the source domain, which must cover those found in the target data to achieve better transfer results in the target domain. To address this issue, current research is exploring methods such as assigning multiple sublabel dictionaries to samples capable of expressing their features to describe unknown faults or using adversarial learning methods to identify such faults. These are directions for future research.

ACKNOWLEDGMENT

Declaration of competing interest:

The authors declare that they have no known competing financial interests or personal relationships that could have appeared to influence the work reported in this paper.

REFERENCES

[1] N. Zhao, J. Zhang, W. Ma, Z. Jiang, and Z. Mao, "Variational time-domain decomposition of reciprocating machine multi-impact vibration signals," *Mech. Syst. Signal Process.*, vol. 172, Jun. 2022, Art. no. 108977, doi: 10.1016/j.ymssp.2022.108977.

[2] M. Wang, J. Guo, Q. Peng, and S. Cao, "Research on fault feature extraction of diesel engine cylinder based on MMD and KICA," in *Proc. Int. Conf. Intell. Manuf., Adv. Sens. Big Data (IMASBD)*, Guilin, China, Jul. 2022, pp. 44–50, doi: 10.1109/IMASBD57215.2022.00014.

[3] Y. Ke, E. Song, Y. Chen, C. Yao, and Y. Ning, "Multiscale bidirectional diversity entropy for diesel injector fault-type diagnosis and fault degree diagnosis," *IEEE Trans. Instrum. Meas.*, vol. 71, 2022, Art. no. 6503410, doi: 10.1109/TIM.2022.3218329.

[4] M. T. Chaichan, "Combustion and emission characteristics of E85 and diesel blend in conventional diesel engine operating in PPCI mode," *Thermal Sci. Eng. Prog.*, vol. 7, pp. 45–53, Sep. 2018, doi: 10.1016/j.tsep.2018.04.013.

[5] D. Tang, F. Bi, J. Lin, X. Li, X. Yang, and X. Bi, "Adaptive recursive variational mode decomposition for multiple engine faults detection," *IEEE Trans. Instrum. Meas.*, vol. 71, 2022, Art. no. 3513111, doi: 10.1109/TIM.2022.3173646.

[6] Z. Feng, D. Zhang, and M. J. Zuo, "Adaptive mode decomposition methods and their applications in signal analysis for machinery fault diagnosis: A review with examples," *IEEE Access*, vol. 5, pp. 24301–24331, 2017, doi: 10.1109/ACCESS.2017.2766232.

[7] X. Xu, X. Yan, C. Sheng, C. Yuan, D. Xu, and J. Yang, "A belief rule-based expert system for fault diagnosis of marine diesel engines," *IEEE Trans. Syst., Man, Cybern., Syst.*, vol. 50, no. 2, pp. 656–672, Feb. 2020, doi: 10.1109/TSMC.2017.2759026.

[8] X. Bi, J. Lin, F. Bi, X. Li, D. Tang, Y. Wu, X. Yang, and P. Shen, "Engine working state recognition based on optimized variational mode decomposition and expectation maximization algorithm," *IEEE Access*, vol. 8, pp. 33545–33559, 2020, doi: 10.1109/ACCESS.2020.2975113.

[9] Q. Chu, J. Huang, and S. Ren, "Multi-condition fault diagnosis of internal combustion engine based on convolutional network," in *Proc. 6th Int. Symp. Comput. Sci. Intell. Control (ISCSIC)*, Beijing, China, Nov. 2022, pp. 166–170, doi: 10.1109/ISCSIC57216.2022.00043.

[10] J. Liang, Z. Mao, F. Liu, X. Kong, J. Zhang, and Z. Jiang, "Multi-sensor signals multi-scale fusion method for fault detection of high-speed and high-power diesel engine under variable operating conditions," *Eng. Appl. Artif. Intell.*, vol. 126, Nov. 2023, Art. no. 106912, doi: 10.1016/j.engappai.2023.106912.

[11] Y. Xie, T. Niu, S. Shao, Y. Zhao, and Y. Cheng, "Attention-based convolutional neural networks for diesel fuel system fault diagnosis," in *Proc. Int. Conf. Sens., Meas. Data Anal. Era Artif. Intell. (ICSMD)*, Oct. 2020, pp. 210–214, doi: 10.1109/ICSMD50554.2020.9261700.

[12] R. Wang, H. Chen, and C. Guan, "DPGCN model: A novel fault diagnosis method for marine diesel engines based on imbalanced datasets," *IEEE Trans. Instrum. Meas.*, vol. 72, 2023, Art. no. 3504011, doi: 10.1109/TIM.2022.3228002.

[13] G. Xiong, W. Ma, N. Zhao, J. Zhang, Z. Jiang, and Z. Mao, "Multi-type diesel engines operating condition recognition method based on stacked auto-encoder and feature transfer learning," *IEEE Access*, vol. 9, pp. 31043–31052, 2021, doi: 10.1109/ACCESS.2021.3057399.

[14] A. Huang, B. Bao, N. Zhao, J. Zhang, Z. Jiang, and Z. Mao, "Decoupling identification method of continuous working conditions of diesel engines based on a graph self-attention network," *IEEE Access*, vol. 10, pp. 36649–36661, 2022, doi: 10.1109/ACCESS.2022.3164077.

[15] D. Zhao, L. Cui, and F. Chu, "Scaling demodulation-based mode decomposition for analyzing nonstationary signal with close-spaced and intersecting frequency trajectories," *Measurement*, vol. 203, Nov. 2022, Art. no. 112007, doi: 10.1016/j.measurement.2022.112007.

[16] S. Niu, Y. Liu, J. Wang, and H. Song, "A decade survey of transfer learning (2010–2020)," *IEEE Trans. Artif. Intell.*, vol. 1, no. 2, pp. 151–166, Oct. 2020, doi: 10.1109/TAI.2021.3054609.

[17] Z.-H. Liu, B.-L. Lu, H.-L. Wei, L. Chen, X.-H. Li, and M. Rätsch, "Deep adversarial domain adaptation model for bearing fault diagnosis," *IEEE Trans. Syst., Man, Cybern., Syst.*, vol. 51, no. 7, pp. 4217–4226, Jul. 2021, doi: 10.1109/TSMC.2019.2932000.

[18] W. Mao, Y. Liu, L. Ding, A. Safian, and X. Liang, "A new structured domain adversarial neural network for transfer fault diagnosis of rolling bearings under different working conditions," *IEEE Trans. Instrum. Meas.*, vol. 70, pp. 1–13, 2021, doi: 10.1109/TIM.2020.3038596.

[19] Z. Tong, W. Li, B. Zhang, F. Jiang, and G. Zhou, "Bearing fault diagnosis under variable working conditions based on domain adaptation using feature transfer learning," *IEEE Access*, vol. 6, pp. 76187–76197, 2018, doi: 10.1109/ACCESS.2018.2883078.

[20] X. Yu, Z. Zhao, X. Zhang, C. Sun, B. Gong, R. Yan, and X. Chen, "Conditional adversarial domain adaptation with discrimination embedding for locomotive fault diagnosis," *IEEE Trans. Instrum. Meas.*, vol. 70, pp. 1–12, 2021, doi: 10.1109/TIM.2020.3031198.

[21] B. Wang, Y. Wei, S. Liu, D. Zhao, and X. Liu, "Unsupervised joint sub-domain adaptation network for fault diagnosis," *IEEE Sensors J.*, vol. 22, no. 9, pp. 8891–8903, May 2022, doi: 10.1109/JSEN.2022.3163425.

[22] I. Titov, "Domain adaptation by constraining inter-domain variability of latent feature representation," in *Proc. 49th Annu. Meeting Assoc. Comput. Linguistics, Human Lang. Technol.*, 2011, pp. 62–71.

[23] L. Zhang, H. Li, J. Cui, W. Li, and X. Wang, "Class subdomain adaptation network for bearing fault diagnosis under variable working conditions," *IEEE Trans. Instrum. Meas.*, vol. 72, pp. 1–17, 2023, doi: 10.1109/TIM.2022.3230479.

[24] W. Lu, B. Liang, Y. Cheng, D. Meng, J. Yang, and T. Zhang, "Deep model based domain adaptation for fault diagnosis," *IEEE Trans. Ind. Electron.*, vol. 64, no. 3, pp. 2296–2305, Mar. 2017, doi: 10.1109/TIE.2016.2627020.

[25] Y. Shen, B. Chen, F. Guo, W. Meng, and L. Yu, "A modified deep convolutional subdomain adaptive network method for fault diagnosis of wind turbine systems," *IEEE Trans. Instrum. Meas.*, vol. 71, pp. 1–10, 2022, doi: 10.1109/TIM.2021.3128708.

[26] S. Li, Z. An, and J. Lu, "A novel data-driven fault feature separation method and its application on intelligent fault diagnosis under variable working conditions," *IEEE Access*, vol. 8, pp. 113702–113712, 2020, doi: 10.1109/ACCESS.2020.2996713.

[27] R. Huang, H. Sun, J. Liu, L. Tian, L. Wang, Y. Shan, and Y. Wang, "Feature variance regularization: A simple way to improve the generalizability of neural networks," in *Proc. AAAI Conf. Artif. Intell.*, vol. 34, 2020, pp. 4190–4197, doi: 10.1609/aaai.v34i04.5840.

[28] Y. Cai, Z. Xu, Q. Wen, J. Shi, F. Zhong, X. Yang, J. Yang, and H. Zhou, "Fault states diagnosis of marine diesel engine valve based on a modified VGG16 transfer learning method," *Math. Problems Eng.*, vol. 2023, pp. 1–14, May 2023, doi: 10.1155/2023/1225536.

[29] T. Jian, H. Huijuan, S. Gehao, and J. Xiuchen, "Transformer fault diagnosis model with unbalanced samples based on SMOTE algorithm and focal loss," in *Proc. 4th Int. Conf. Energy, Electr. Power Eng. (CEEPE)*, Chongqing, China, Apr. 2021, pp. 693–697, doi: 10.1109/CEEPE51765.2021.9475723.

HE LI received the B.S. degree from Beijing University of Chemical Technology, in 2019, where he is currently pursuing the Ph.D. degree. His current research interest includes intelligent fault diagnosis of reciprocating machinery, mainly for diesel engines and reciprocating compressors.

LIANGYU DONG is currently an Engineer with China Industrial Control Systems Cyber Emergency Response Team. Her research interests include network security, industrial control security, industrial internet security, and data security.

YANG PENG is currently with the Gathering and Transportation Engineering Technology Research Institute, PetroChina Southwest Oil and Gasfield Company. His main research interests include equipment intelligent operation and maintenance, monitoring, and diagnosis.

ZHIXIANG DAI is currently a Senior Engineer mainly engaged in research on surface construction and oil and gas storage and transportation engineering in oil and gas fields, and equipment management in oil and gas fields.

YANG JIANG received the bachelor's degree in oil and gas storage and transportation from Southwest Petroleum University. He is currently an Oil and Gas Storage and Transportation Engineer and a Political Engineer.

JINJIE ZHANG received the Ph.D. degree from Beijing University of Chemical Technology, in 2014. He stayed with Beijing University of Chemical Technology the Ph.D. degree, in 2016. He engaged in research on online monitoring and intelligent diagnosis technology of reciprocating machinery faults, he has published more than 20 articles in the field of fault monitoring and diagnosis of reciprocating compressors, won three provincial and ministerial level scientific and technological progress awards, and nine authorized invention patents.